J Mol Model (2011) 17:817–831
DOI 10.1007/s00894-010-0752-2

ORIGINAL PAPER

Design of 1-arylsulfamido-2-alkylpiperazine derivatives as secreted PLA_2 inhibitors

Preethi Badrinarayan · P. Srivani · G. Narahari Sastry

Received: 1 March 2010 / Accepted: 11 May 2010 / Published online: 23 June 2010

Abstract Structure and analog based analysis of 3D-QSAR, CoMFA and CoMSIA, along with different docking protocols were used to evaluate the structure activity relationship of 26 analogues of 1-aryl sulfamido-2-alkyl piperazines to model the activities of group I and II secreted phospholipases A_2 ($sPLA_2$s) and probe into the chemical space and nature of receptor — ligand interactions. The best CoMFA model yields cross-validated (q^2) and conventional correlation coefficients (r^2) of 0.703 and 0.962 respectively whereas CoMSIA model yields q^2 and r^2 values of 0.408 and 0.922 respectively, followed by docking analysis using FlexX and GOLD methodologies on the X-ray structure of human and bovine PLA_2s. A comparative study was made to find out the differences in the active site residues of both PLA_2s. The information enunciated from the analysis of CoMFA and CoMSIA maps and docking results were analyzed and employed in the design of 29 new ligands using molecules **4**, **21**, **22** from the initial set as templates. New ligands for group I and II secreted phospholipases A_2 ($sPLA_2$s) have been thus designed based on the 32 analogues of 1-aryl sulfamido-2-alkyl piperazine with a cursory note on its synthetic feasibility. Molecular modeling studies indicate that the newly designed ligands are expected to show high affinity and experimental efforts in this direction is highly rewarding.

Keywords CoMFA · CoMSIA · Docking · Design · Molecular modeling · PLA_2

Introduction

Phospholipase A_2 (PLA_2) belongs to a class of enzyme that specifically catalyze the hydrolysis of membrane glycerophospholipids at the sn-2 position with the liberation of free fatty acids (arachidonic acid, AA) and lysophospholipids. These metabolites in turn serve as substrates for the biosynthesis of prostaglandins, thromboxanes, leukotrienes and other oxygenated metabolites of AA (*i.e.*, eicosanoids) in addition to another proinflamatory mediator namely platelet activating factor on enzymatic acetylation of lysophospholipid. These products play an important role in transmembrane signaling and cause inflammation. The 14 KDA $sPLA_2$s which constitute the large class of PLA_2 enzymes have been classified into three main groups (I, II and III) based on the similarities derived in their primary sequences [1, 2]. Recent cloning strategies have revealed several new $sPLA_2$s representing ten different groups [3]. PLA_2s are a diverse class of enzymes with regard to function, localization, regulation, mechanism, sequence, structure, and role of divalent metal atoms [4]. A target specific research aimed to generate potential 'leads' for PLA_2s finally resulted in the generation of various 'new ligands' as potential PLA_2 inhibitors.

Increased enzymatic activity of human non pancreatic secretary PLA_2 triggers a number of disease states such as rheumatoid arthritis, septic shock and atherosclerosis and many other chronic disorders like asthma, psoriasis, Crohn's disease and ulcerative colitis [5–8]. PLA_2 also exhibits a vital role in the regulation of cyclooxygenase (COX) and 5-lipooxygenase (5-LO) pathways that mediate

Electronic supplementary material The online version of this article (doi:10.1007/s00894-010-0752-2) contains supplementary material, which is available to authorized users.

P. Badrinarayan · P. Srivani · G. Narahari Sastry (✉)
Molecular Modeling Group, Organic Chemical Sciences,
Indian Institute of Chemical Technology,
Tarnaka Hyderabad 500 007, India
e-mail: gnsastry@gmail.com

inflammatory reactions. It has therefore been treated as a potent therapeutic target to reduce inflammation.

Very few $sPLA_2$s inhibitors have been accredited to date constituting structurally different scaffolds *viz.* γ—hydroxy butenolides, oxazolidinones, dystronic acids and others [9–12]. Amidst these different scaffolds specified, a series of indole derivatives specifically inhibited $snpPLA_2$ was reported in 1995 [13–16]. The present paper reports 3D-QSAR and docking studies of 1-arylsulfamido-2-alkylpiperazines [17–20], which were reported as strong inhibitors for group I and II $sPLA_2$s. The 29 new ligands were designed based on meticulous perusal of the observations deduced from QSAR and docking analysis.

In continuation to our efforts in the area of computer aided drug design [22–26] both QSAR and docking protocols were chosen to construct a reliable protein-ligand complex. Problems during the alignment procedure precluded the inclusion of all 32 molecules in QSAR studies therefore only 26 molecules were considered in the initial set. Molecule **32** had to be designated as an outlier as it comprised of 16 carbon atoms, compared to 9–12 observed in most molecules, with poor IC_{50} value. Comparative molecular field analysis (CoMFA) has emerged as an efficient 3D-QSAR tool which effectively correlates the changes in biological activities with variation in the steric and electrostatic fields of the molecules exemplified at lattice points of 3D. Analysis of the CoMFA and CoMSIA maps revealed specific locations in the regions occupied by the ligands that tend to favor or disfavor the presence of a group imparting a specific physicochemical property. Following this correlation can be obtained between the field parameters and biological activity of a compound which attributes the contribution of H-bonding interactions to the disparities in the inhibitory activities amidst compounds. The observations which are subsequently associated with the variations in molecular fields at specific regions of the space correlate to the biological activities and specify the structural requirements of the Group I and II $sPLA_2$s. These observations were incorporated in the design of new leads with the rational application of molecular modeling tools.

Docking studies were carried out by employing the FlexX module in SYBYL 6.9 [27, 28], and GOLD version 2.2 [29, 30] with 26 analogues of piperazines onto the active sites of both bovine pancreatic PLA_2 as well as human PLA_2. The docking results provide comparative analysis with respect to binding affinities being drawn as well as ligand-receptor specificity being exemplified.

Docking results were analyzed to probe into the active site of $sPLA_2$s extricating intricate details on the interactions of receptor-ligand complex, chemical space and nature. These results are also useful for structural modifications of known ligands and/or to design new ligands with the aid of virtual screening [31].

Computational details

Dataset for analysis

Reported *in vitro* data [17] of 32 molecules was considered for the present study (Table 1). The reported IC_{50} values (experimental activity) of the dataset against bovine pancreatic PLA_2 ranged from 1.4 to 100 μM, and were converted to the corresponding pIC_{50} values. The following formula was used for the conversion of IC_{50} to pIC_{50}.

$$pIC_{50} = -\log IC_{50}$$

Molecular modeling

All calculations and simulations were run on a PC under Linux. The 3D-QSAR studies were carried out using SYBYL and the docking studies using FlexX and GOLD. All the molecules were minimized using Tripos force field and Gasteiger-Hückel partial atomic charges implementing Powell's conjugate gradient method with a distance dependent dielectric constant, until a convergence gradient of 0.001 kcal mol^{-1} was accomplished. Since the N atom of the piperzine ring is basic in nature and is protonated at the physiological pH, the piperzine ring was considered in the protonated form [32–34].

3D-QSAR

The entire set of $sPLA_2$s inhibitors comprised of 32 compounds out of which only 26 compounds were considered. The test and training sets were selected so as to include structurally diverse analogues in the set with pIC_{50} values ranging from high to low.

Alignment

The alignment of structures was the most subjective and imperative step in CoMFA analysis, as the 3D — QSAR model built was often sensitive to specific alignment layout. The sensitivity of CoMFA models to alterations in orientation of the superimposed molecules in the 3D lattice space enabled the implementation of various alignment schemes. Two alignment protocols in SYBYL were used: (1) database alignment method, which does not alter the orientation of the molecules, and (2) RMS fit, which was designated by the root mean square deviation (RMSD)

Table 1 Dataset considered in the present analysis and the experimental activities (IC_{50}) of the data are provided in μM units

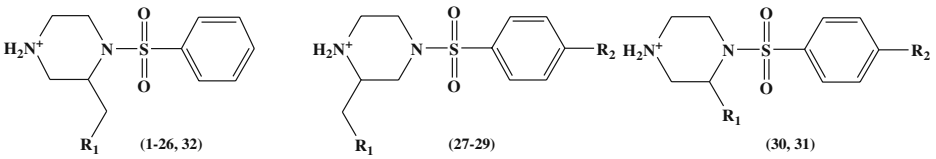

S. No	R_1	R_2	IC_{50}	S. No	R_1	R_2	IC_{50}
1	nC_5H_{11}	*p*-CH_3	100	**17**	7(Z)$nC_{12}H_{23}$	*p*-OCH3	3.80
2	nC_7H_{15}	*p*-CH_3	17.30	**18**	7(E)$nC_{12}H_{23}$	*p*-OCH_3	2.30
3	nC_9H_{19}	*p*-CH_3	8.80	**19**	$nC_{12}H_{25}$	*p*-Br	5.40
4	$nC_{12}H_{25}$	*p*-CH_3	2.45	**20**	$nC_{12}H_{25}$	*p*-NH_2	2.00
5	$nC_{14}H_{29}$	*p*-CH_3	9.00	**21**	$nC_{12}H_{25}$	*p*-$N(CH_3)_2$	1.40
6	nC_7H_{15}	*p*-H	19.30	**22**	$nC_{12}H_{25}$	*p*-$NHCOCH_3$	2.20
7	nC_7H_{15}	*p*-SO_2CH_3	51.25	**23**	$nC_{12}H_{25}$	*p*-$NHCO_2Et$	2.20
8	nC_7H_{15}	*p*-Cl	16.70	**24**	$nC_{12}H_{25}$	*p*-$NHCOC_6H_5$	2.50
9	nC_7H_{15}	*p*-OCH_3	10.00	**25**	$nC_{12}H_{25}$	*p*-$CH(CH_3)_2$	100
10	nC_7H_{15}	*o*-OCH_3	37.70	**26**	$nC_{12}H_{25}$	*p*-CH_2CH_3	100
11	nC_7H_{15}	*m*-OCH_3	17.00	**27**	nC_9H_{19}	*p*-CH_3	12.10
12	nC_7H_{15}	3,4,5-triOCH_3	33.80	**28**	$nC_{12}H_{25}$	*p*-CH_3	5.50
13	$nC_{12}H_{25}$	*p*-H	8.00	**29**	$nC_{14}H_{29}$	*p*-CH_3	6.80
14	$nC_{12}H_{25}$	*p*-SO_2CH_3	3.00	**30**	(R)$CH_2OC_{14}H_{29}$	*p*-OCH_3	2.76
15	$nC_{12}H_{25}$	*p*-Cl	7.50	**31**	(S)$CH_2OC_{14}H_{29}$	*p*-OCH_3	2.90
16	$nC_{12}H_{25}$	*p*-OCH_3	1.90	**32**	$nC_{16}H_{33}$	*p*-CH_3	80.00

value, figured out for analogous atoms. The most active compound **21** was used as a template to build the data set conformations as well as for the alignment. The aligned molecules are as shown in Fig. 1.

Generation of CoMFA and CoMSIA fields

The CoMFA and CoMSIA fields were calculated using the same protocols employed in our earlier studies [21–26]. The statistical model was constructed using PLS regression procedure

Docking

As mentioned earlier, the docking studies were performed using two different methods, GOLD version 2.2 and FlexX for all the 26 molecules and for newly designed compounds. The ligands were docked into the active sites of both bovine and human $sPLA_2$s and a comparative analysis of binding affinities was done. The crystal structures of bovine $sPLA_2$s (PDB code: 1KVX) and human PLA_2 complexed with indole 8 (PDB code 1DB4) were downloaded from the Brookhaven Protein Data Bank (http://www.rcsb.org). All the hydrogens were added using the Biopolymer module in SYBYL. Using the Tripos force field and Kollman-All partial atomic charges for the protein minimization where +2 charge was assigned for the calcium atom and all the non-hydrogens were aggregated during the minimization. Powell's conjugate gradient method with distance dependent dielectric constant value of 1.0 and a gradient convergence value of 0.05 kcal mol^{-1} was used for minimization. For GOLD docking, the active sites with 8 Å radius sphere from His48 backbone nitrogen for bovine and from oxygen of Tyr51 phenyl ring for human were defined. The 10 best conformations were considered for binding mode analysis on basis of GOLD Score. In FlexX, the active site comprise of an 8 Å sphere from the calcium atom, His48 and Tyr51 residues (the residues numbers were given with respect to bovine PLA_2 and for human the corresponding residues were used), following the FlexX

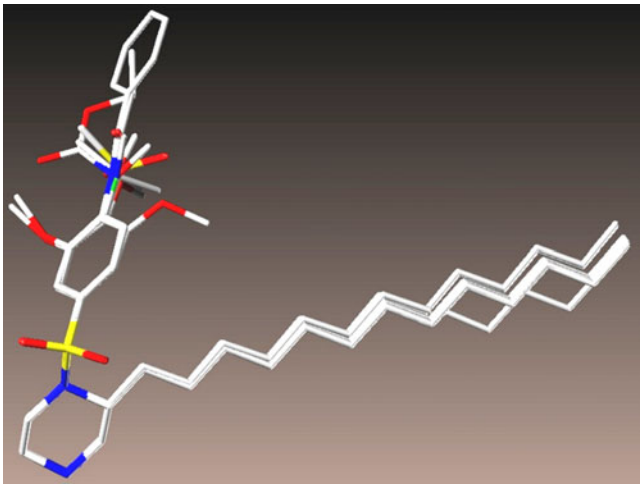

Fig. 1 Alignment of dataset molecules used to build the QSAR model

score the top 30 conformations were saved for further binding mode analysis.

Results and discussion

This section presents, first the results of CoMFA and CoMSIA models, followed by the discussion of contour maps based on the assumption that the changes in binding affinities of ligands are related to the changes in molecular properties represented by maps. The analysis of the docked molecules has also been summarized in this section providing a detailed report about the variations in binding affinity with respect to ligand-receptor specificities.

CoMFA results

Initially, a total of 32 molecules were considered for CoMFA analysis but five (**27–31**) molecules had to be eliminated due to alignment setbacks and molecule **32** with a long 16-carbon chain length could not be considered as well. Therefore, only 26 molecules were included for the 3D-QSAR analysis. The CoMFA model was obtained with 20, 1-arylsulfamido-2-alkylpiperazine analogues in the training set with other six compounds catering for the test set obtained through database alignment, resulting in a cross-validated correlation coefficient of 0.703 and minimum standard error of prediction value (SEP) of 0.379. The conventional QSAR run was pursued with the optimum components that were obtained from the previous analysis giving a correlation coefficient of 0.962 with a satisfactory standard error of

Table 2 Summary of CoMFA and CoMSIA studies, the values in italic represents the dataset summary without considering the alkylpiperazine ring in protonated form

Parameter	CoMFA	CoMSIA			
		Model 1[f]	Model 2[g]	Model 3[h]	Model 4[i]
r^2	0.962 *0.941*	0.922	0.891	0.925	0.843
q^2	0.703 *0.629*	0.408	0.405	0.333	0.383
N	4 *5*	7	5	7	6
SEE	0.136 *0.175*	0.218	0.238	0.213	0.296
SEP	0.379 *0.439*	0.598	0.556	0.635	0.587
F	94.48 *44.61*	20.13	22.85	21.12	8.94
PRESS	0.27 *0.23*	–	–	–	–
r_{pred}^2	0.795 *0.817*	–	–	–	–
% of field contributions					
S[a]	59.6 *61.3*	21.7	27.1	34.4	–
E[b]	40.4 *38.7*	32.4	36.0	41.0	–
H[c]	–	29.1	36.9	–	63.5
D[d]	–	02.9	–	05.7	13.2
A[e]	–	13.9	–	18.9	23.3

[a] steric
[b] electrostatic
[c] hydrophobic
[d] hydrogen bond donor
[e] hydrogen bond acceptor
[f] model built with S, E, H, D & A fields;
[g] model built with S, E & H fields;
[h] model built with S, E, D & A fields;
[i] model built with H, D & A fields;

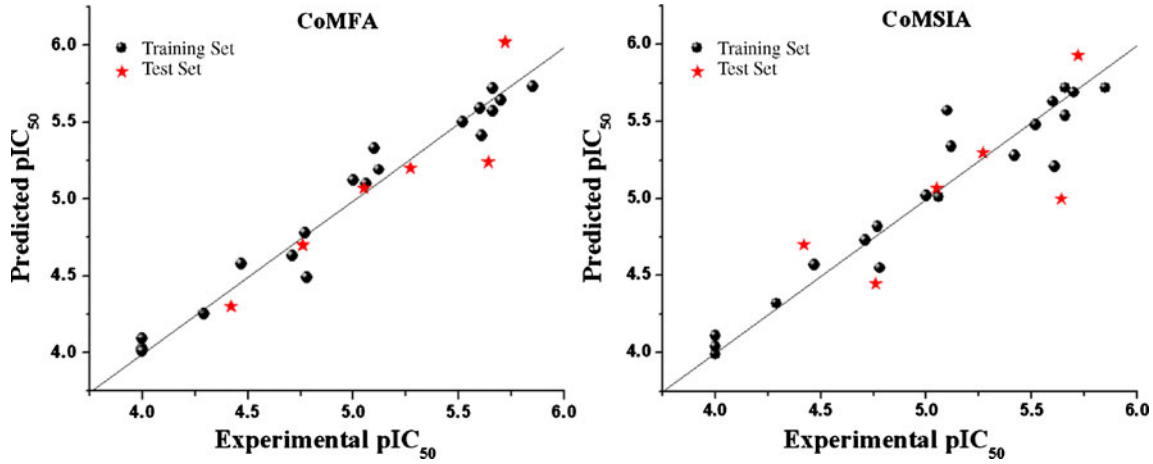

Fig. 2 Graph of experimental *vs*. predicted inhibitor activities of training and test sets for CoMFA and CoMSIA (model 1)

estimate (SEE) of 0.136, PRESS value of 0.27 and predicted r^2 of 0.795, thereby giving a considerably good correlation between the observed and predicted activities of the test set molecules. The predicted and experimental pIC_{50} values for training and test sets are given in Table 2 and plot is illustrated in Fig. 2. The contributions of the CoMFA field descriptors are shown in Fig. 3.

CoMSIA results

Four different CoMSIA models were generated with the combination of five CoMSIA field descriptors by implementing the database alignment method. Among the four models, one model (model 1) was selected for further analysis as the model represented the optimum descriptor information (Table 3). The PLS analysis of model 1 was produced a q^2 of 0.408 with optimum number of seven components and the corresponding r^2 of 0.922 with SEE value of 0.218. The other CoMSIA models 2, 3 and 4 produced also gave considerably good q^2 and r^2 values (Table 2).

Analysis of CoMFA and CoMSIA maps

All the analogues have a hydrophobic chain of length C_5 to C_{16} attached to a piperazine ring which is connected to a sulfurdioxide moiety and the group in turn to a phenyl ring embraces various *para* (23 molecules), *ortho* (1 molecule) and *meta* (1 molecule) substituents. The CoMFA contour map analysis (Figs. 3 and 4) reveal that the hydrophobic part of the series is having a green contour in the middle and small yellow contours at the end of the chain indicating for the optimal chain length required for PLA_2 activity. The compounds with C_{14} (**5**) and C_{16} (**32**) chain tend to decrease the IC_{50} as well as the q^2 and r^2 values of the CoMFA model (data not shown). Therefore, we infer from the green contour that the optimum chain length may perhaps be between C_9 to C_{12} as in compounds **16–18** and **20–24** for good potency and

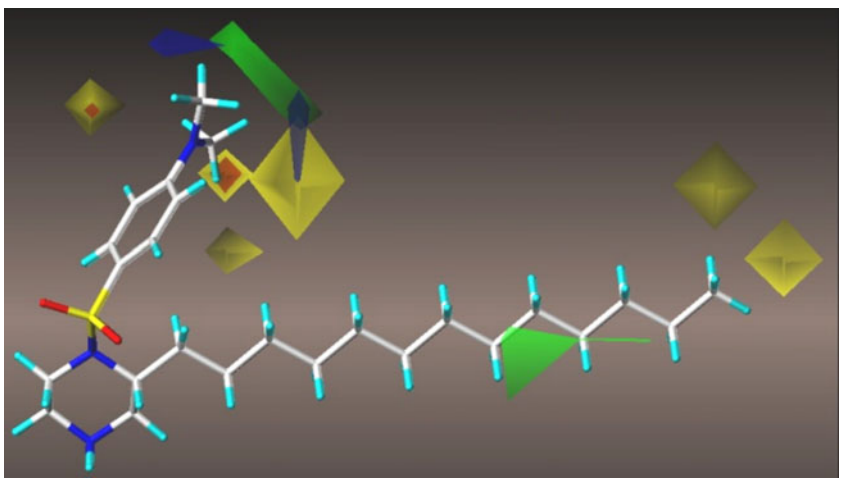

Fig. 3 CoMFA steric and electrostatic STDEV*COEFF contour maps, the template molecules are displayed in the background. The color representation is as follows: green (favored) and yellow (disfavored) for steric, blue (electropositive) and red (electronegative) for electrostatic

Table 3 Experimental and predicted inhibitory activities (pIC_{50}) and residuals of both training and test sets (*) for CoMFA and CoMSIA

Compd. No.	Experimental activity	Predicted activity		Residuals	
		CoMFA	CoMSIA[a]	CoMFA	CoMSIA[a]
1	4.00	4.03	3.99	−0.03	0.01
2*	4.76	4.70	4.45	0.06	0.31
3	5.06	5.10	5.01	−0.04	0.05
4	5.61	5.41	5.21	0.20	0.40
5*	5.05	5.07	5.07	−0.02	−0.02
6	4.71	4.63	4.73	0.08	−0.02
7	4.29	4.25	4.32	0.04	−0.03
8	4.78	4.49	4.55	0.29	0.23
9	5.00	5.12	5.02	−0.12	−0.02
10*	4.42	4.30	4.70	0.12	−0.28
11	4.77	4.78	4.82	−0.01	−0.05
12	4.47	4.58	4.57	−0.11	−0.10
13	5.10	5.33	5.57	−0.23	−0.47
14	5.52	5.50	5.48	0.02	0.04
15	5.12	5.19	5.34	−0.07	−0.22
16*	5.72	6.02	5.93	−0.30	−0.21
17	5.42	5.56	5.28	−0.14	0.14
18*	5.64	5.24	5.00	0.40	0.64
19*	5.27	5.20	5.30	0.07	−0.03
20	5.70	5.64	5.69	0.06	0.01
21	5.85	5.73	5.72	0.12	0.13
22	5.66	5.72	5.72	−0.06	−0.06
23	5.66	5.57	5.54	0.09	0.12
24	5.60	5.59	5.63	0.01	−0.03
25	4.00	4.09	4.04	−0.09	−0.04
26	4.00	4.01	4.11	−0.01	−0.11

[a] values are predicted using Model 1

if decreased as in compounds **1** and **2** having C_5 and C_7 the potency worsens. The electrostatic blue and red contours, which enclose R_2 position, infer that an electrostatic group may possibly increase the activity. The presence of sulfur as sulfates (**14**) oxygen as methoxy group (**16–18**) and nitrogen as primary amine, disubstituted amine and amides (**20–24)** showed that electrostatic groups aid to increase the activity. The compounds **25** and **26** devoid of electrostatic groups show least activity as expected. Yellow contours near the R_2 position are steric unfavorable as evident by the lower activities for compounds **25** and **26**. Compounds **6–9** and **13–16** do not follow the above trend which is explained based on the analysis given below.

The compounds **6–9** contain identical electrostatic groups with compounds **13–16**, however the similarity is not observed in terms of activity. This can be attributed to the hydrophobic chain length where the second series (**13–16)** holds a C_{12} chain and the first series (**6–9**) possesses a C_7 chain. On the other hand the molecules **25** and **26** are not active even though they have C_{12} chain, lack of electrostatic group at R_2 position might be the reason for such a low activity! Surprisingly, compound **4** does not have any electrostatic group at R_2 but exhibits comparable activity. From this analysis one can suggests that perhaps the chain length controls the electrostatic interactions and the interactions are optimum with C_{12} and gradually decreases from C_9 to C_7 to C_5 and so on. To see how this chain length tunes the electrostatic interactions and how the interactions in turn play a crucial role for the activity, these 26 compounds were docked in the active site of bovine and human PLA_2.

CoMSIA maps provided information about hydrophobic and hydrogen bonding parameters. The orange (hydrophobic favorable) region surrounding the carbon chain strongly supports the CoMFA green contour analysis, which conveys that the optimum carbon chain length should be most likely between C_9 to C_{12}. The white (hydrophobic unfavorable) contour near the *para* substituent of phenyl group signifies that hydrophilic groups are favorable, which in turn supports the CoMFA yellow contour as well as electrostatic contours. The hydrophobic region unequivocally infers that the optimal length of the carbon chain (C_9–C_{12}) is obligatory

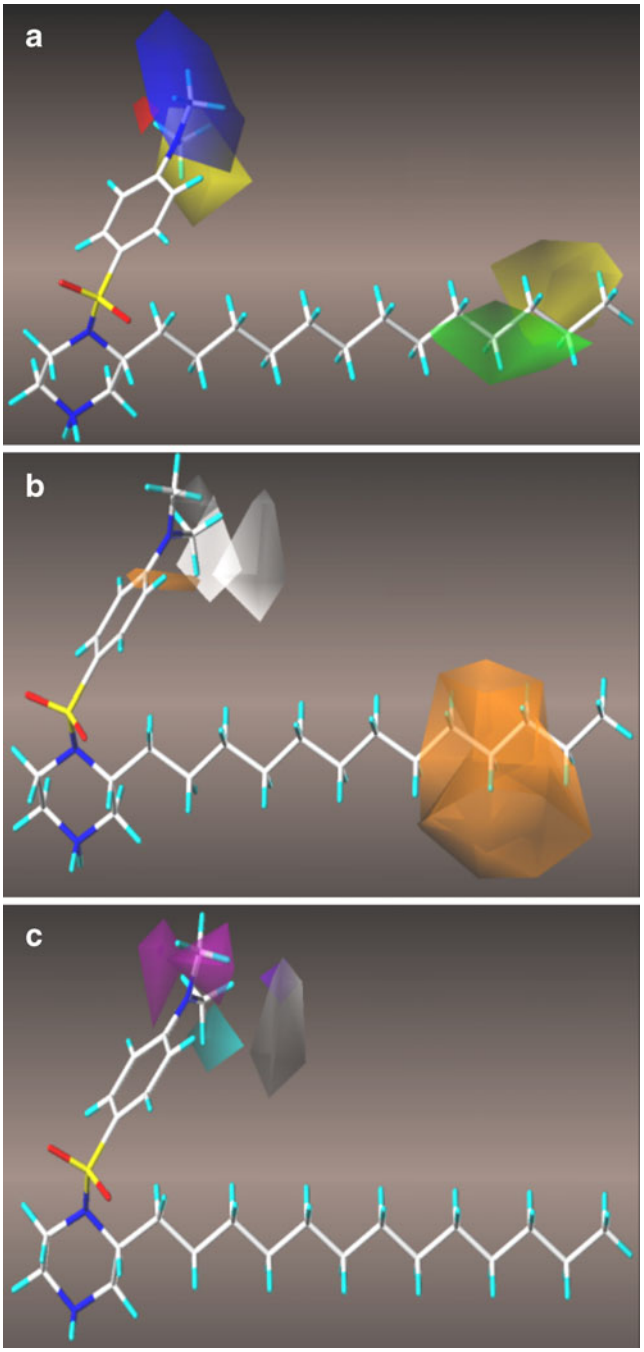

Fig. 4 CoMSIA contour maps steric and electrostatic (**a**), hydrophobic, donor and acceptor (**b**) fields for model. The most active compound **21** is shown in the background. The different colors represent as follows: green (favored) and yellow (disfavored) for steric, blue (electropositive) and red (electronegative) for electrostatic, orange (favored) and white (disfavored) for hydrophobic, cyan (favored) and purple (disfavored) for donor and magenta (favored) and white (disfavored) for acceptor

for electrostatic interactions. The cyan and white color contours near the *para* substituent of phenyl ring (Fig. 4) exemplify that the hydrogen bond donor is more favorable than the acceptor.

Docking analysis

The docking calculations add to the understanding of the structural requirements for binding to the PLA_2 enzyme. In GOLD calculations, only hydrogen bonding interactions and van der Waals interactions were evaluated and electrostatic interactions were not considered whereas FlexX includes both steric as well as electrostatic interactions (Table 4). Since the reported IC_{50} values were against the bovine PLA_2, the corresponding protein was considered for the present docking study but to see how the binding interactions change from bovine to human, human PLA_2 was also considered. The topology of the active site for both the proteins is comparable (Fig. 5). The human (area-564.5 $Å^2$; volume-675.8 $Å^3$) active site is greater in size than the bovine (area-456.8 $Å^2$; volume-547.7 $Å^3$). However, the sequence alignment of bovine and human PLA_2s was done with ClustalW [35] and BLAST (Fig. S1) has revealed that 11 residues out of the 21 active site

Table 4 GOLD and FlexX docking scores for dataset docked in the active sites of bovine and human PLA_2s

Compd. No.	Bovine		Human	
	GOLD	FlexX	GOLD	FlexX
1	51.40	−11.70	45.69	−16.50
2	56.18	−09.80	51.38	−15.90
3	57.66	−08.60	54.95	−14.30
4	62.71	−06.20	55.97	−12.50
5	52.71	−06.10	57.18	−11.00
6	53.50	−13.60	51.29	−11.60
7	54.24	−11.80	52.18	−13.30
8	55.77	−08.70	52.71	−11.60
9	56.13	−09.80	52.57	−15.90
10	54.95	−13.90	51.18	−11.80
11	53.81	−16.60	50.61	−15.60
12	49.37	−10.80	47.85	−13.40
13	59.16	−08.90	53.13	−07.90
14	62.23	−09.30	49.54	−17.10
15	64.95	−05.50	58.46	−07.90
16	56.15	−07.10	49.78	−13.50
17	69.92	−08.50	60.12	−15.30
18	62.07	−09.70	57.89	−15.80
19	61.90	−05.50	52.46	−07.90
20	48.79	−09.40	57.16	−12.20
21	50.57	−09.30	42.53	−10.10
22	53.30	−11.10	56.79	−14.80
23	57.62	−08.60	53.32	−15.50
24	59.40	−21.10	43.30	−18.30
25	57.03	−09.00	55.76	−06.40
26	62.51	−08.00	55.79	−12.00

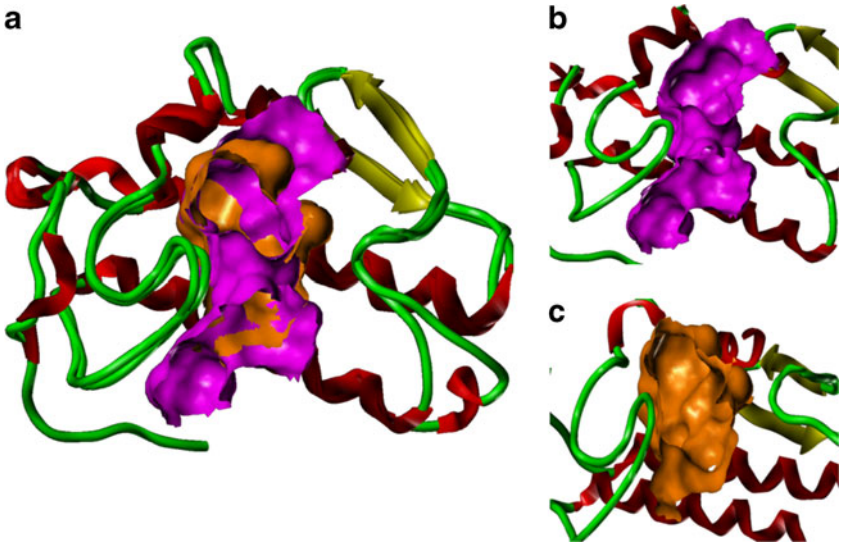

Fig. 5 Overlay of PLA_2s active sites — bovine (orange) and human (magenta) generated by fast Connolly surfaces of SYBYL6.9. The secondary structures are shown as red, yellow and green helices, β-sheets and loops respectively. The human active site (area-564.5; volume-675.8 in $Å^3$) is greater in size than that of bovine (area-456.8; volume-547.7 in $Å^3$). Fig 5 **b** and **c** show active sites of human and bovine respectively

residues are mutated from bovine to human (Fig. 6). Two of the important residues Lys56 and Tyr69 of bovine, which participate in the hydrogen bonding with piperazine ring, are mutated to Glu55 and Lys62 in human PLA_2.

A quick perusal of the GOLD docked structures reflects that the long carbon chain is located in the hydrophobic pocket with the SO_2 group interacting electrostatically with calcium atom with the phenyl ring orienting toward the solvent region. The carbon chain is deeply buried in the hydrophobic pocket formed by the residues Leu2, Phe5, Ile9, Pro18, Leu19, Gly30 and Phe106. The hydrophobic pocket is big enough to accommodate up to C_{12} chain. When the chain length extends to $C_{14–16}$ the molecules were not properly docked into the pocket as a result the orientation of these molecules was different from the other molecules that have shorter chain length ($<C_{14}$). The SO_2 group and the phenyl ring were positioned properly toward Ca and solvent region when the chain length is $C_{9–12}$, in contrast, as the chain length decreases ($C_{5–7}$) or increases ($C_{14–16}$) the two groups were pulled inside or pushed outside the active site thereby losing their corresponding interactions with the protein, which probably lead to lowered activity. The piperazine ring virtually forms two hydrogen bonds (1.60–2.06 Å) with side chain amine group of Leu56 (Lys52 for human PLA_2) and with hydroxyl group of Tyr69 (Glu55 for human PLA_2) (Fig. 7). The oxygen atom of SO_2 group also forms hydrogen bond (1.88–2.7 Å) with backbone NH of Gly32 (Gly31 for human PLA_2) (Fig. 6). All GOLD docked poses of human PLA_2 followed the aforementioned trend whereas FlexX results for both bovine and human deviate from the discussion. Instead of docking in the hydrophobic pocket, the carbon chain oriented toward the solvent region whereas phenylsulfoamido moiety oriented toward the calcium pocket.

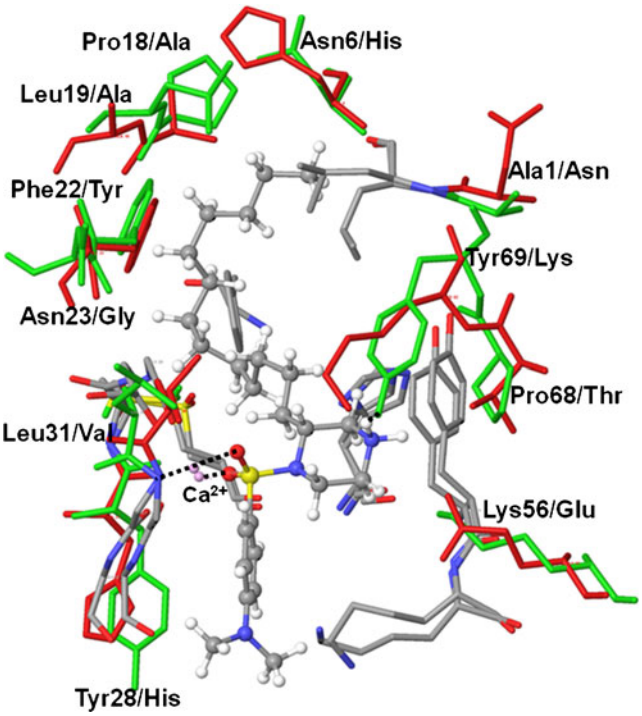

Fig. 6 Active site residues are displayed for both bovine (1KVX) and human (1DB4) $sPLA_2$s. The mutated residues are marked in bold in the table whereas colored green and red for bovine and human respectively in the figure. The hydrogen bonds with Gly32 and Tyr69 (of bovine) and important interactions with Ca^{2+} are showed as black color dotted lines

Combined analysis of QSAR and docking results

Combine analysis of both the methods was done by comparing 3D-QSAR maps with docked poses in the active sites. The resulted 3D maps of both CoMFA and CoMSIA

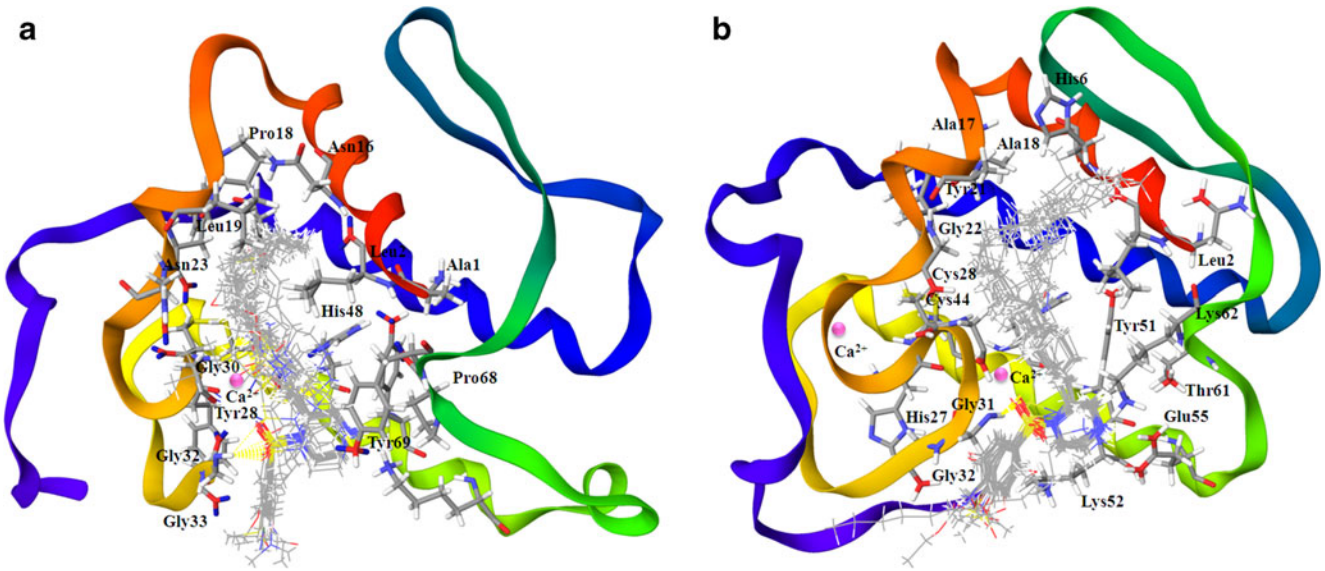

Fig. 7 The docked poses of ligands in the active site of bovine (**a**) and human (**b**). Important hydrophobic residues are shown in capped stick and calcium atom is displayed in pink color ball. Hydrogen bond interactions are presented in yellow color lines

were judged against the corresponding active site residues by directly overlaying them on to the active site. The residues namely, Leu2, Phe5, Ile9, Pro18, Leu19, Gly30 and Phe106, which enclosed the hydrophobic chain, justified the presence of steric favorable green (CoMFA) and hydrophobic (CoMSIA) fields (Fig. 8). The presence of unfavorable steric fields (yellow) around the carbon chain is due to the size of the pocket which can hold only up to C_{12} chain. The electrostatic regions and the hydrogen bond related CoMSIA fields can be associated with the surrounding solvent region of the phenyl group where it might possibly form hydrogen bonds with water. However, all the compounds have similar phenyl, varied hydrophobic (C_{5-16}) side chains and different electrostatic substituents at R_2 position, the appropriate orientation of these groups along with accompanying requirements are necessary for potent inhibitory activity against $sPLA_2$. The docking scores correlate with the IC_{50} values in many instances. Many of the docked conformations are as used for the QSAR model.

Development of strategies for the design of new inhibitors for PLA_2

1. ***Choice of target***: The work presented in the paper enunciates the development of strategies for the *in silico* design of leads by the rational application of different molecular modeling protocols. Our interest and experience in inflammatory diseases along with the therapeutic relevance of $sPLA_2$ inspired us to use this as a study target in the development of strategies for *in silico* lead design.

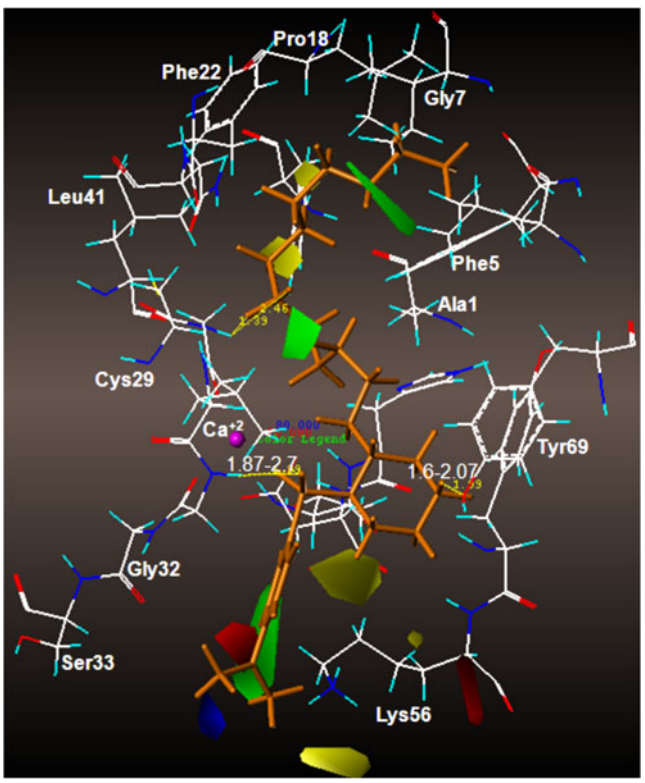

Fig. 8 CoMFA steric and electrostatic fields are projected in the active site of bovine PLA_2. The most active compound **21** is displayed in orange color capped stick. Calcium atom is symbolized in magenta color ball. The green and yellow contours represent steric, blue and red represents electrostatic. Hydrogen bond interactions are shown in yellow color dotted lines and the distances are given

2. ***Choice of basic scaffold***: After a meticulous perusal of the advantages and disadvantages of structurally different classes of sPLA$_2$ inhibitors (γ—hydroxy butenolides, oxazolidinones, dystronic acids), indole derivatives exhibiting good inhibitory activities materialized to be the starting point to initiate the understanding of structure activity relationship.
3. ***3D-QSAR***: The CoMFA and COMSIA generated on doing 3D-QSAR studies explained the status and need of placing electropositive, electronegative, hydrophobic, hydrophilic and steric groups at various positions.
4. ***Docking and active site analysis***: The docking and active site analysis with both bovine and human brought out the point that due to the difference in the size and shape of the active site pocket between bovine and human, the inhibitors of human PLA$_2$ are not buried in the active site unlike bovine. The orientation and binding of the ligands insinuated possibilities of bond formation with slight modifications in R_1 and R_2 positions.
5. ***Inhibitor design***: The combined analysis threw light on a few important aspects which were considered for designing new inhibitors from the present dataset. The observations are as follows:

    a. The optimum carbon chain length (R_1) may preferably be in between C_9–C_{12}. Small alkyl group substitutions are encouraged at 8th, 9th and 10th carbons of R_1.
    b. Possibility of R_2 groups to show hydrogen bonds with Gly31, 32, Glu55 and Lys62.
    c. Possible hydrogen bond interactions for 4th and 6th to 9th carbons of R_1 with Tyr21, Gly29, His47 and Asp48.

As an offshoot of the analysis, three molecules consisting of C_{12} (**4**, **21** and **22**) were taken as templates for design of new ligands. The 29 new ligands were designed (Table 5) by substituting different groups at R_1 and R_2 positions. Meticulous observance of the docked poses of ligands in bovine and human PLA$_2$s explicate that due to the difference in the active site pockets of bovine and human PLA$_2$, the inhibitors were not deeply buried inside the hydrophobic pocket of bovine PLA$_2$ (Fig. 9). The carbon chain of the ligand needs to fold to fit well into the active site cleft of human PLA$_2$ which corroborates well with the CoMSIA steric and electrostatic maps. Accordingly, the carbon chain was substituted with CO, CONH and alkyl groups at 4th, 6th to 8th positions. These newly designed ligands were docked with both bovine and human PLA$_2$s using GOLD docking protocol.

Three different groups namely, alkyl, hydrogen bond donors and acceptors were used as substituent for R_1 and R_2 positions of the templates (Table 5). Encouragingly, the docked poses of the newly designed ligands showed much improved binding with optimal interactions. The alkyl groups, methyl and ethyl show steric interactions with Leu2, Asn6, Ile9, Pro18 and Leu19 of bovine PLA$_2$. Hydrogen bonds were noticed between CO groups substituted at C4 and C6 of R_1 and His47 and Gly29 residues of human PLA$_2$, which were not observed in the initial dataset (Fig. 10). The new R_2 substitutions have shown hydrogen bonds with the backbone of Gly32 of human PLA$_2$ (Fig. 11). The ligands substituted with both alkyl and hydrogen bond donors and acceptors at R_1 show improved binding interactions compared to other designed ligands and templates. The newly designed molecule (**4AIII**) scored better over the initial set and newly designed set (Table 6).

6. ***Evaluation:*** The validation of the designed inhibitor was done *in silico* by docking these inhibitors onto the active site of PLA$_2$ to evaluate the orientation, binding and interactions of the designed inhibitors with the active pocket as compared to the molecules of previous dataset. The resulted 3D maps of both CoMFA and CoMSIA were judged against the corresponding active site residues by directly overlaying them on to the active site along with the docked inhibitors to correlate and compare the contribution of different fields (steric, electrostatic) generated by CoMFA and CoMSIA with the interactions shown by the different groups of the inhibitors on docking. As anticipated, improvement in binding with increase in the number of interactions contributed majorly by the substitutions on C_4 and C_6 made at the alkyl chain was observed. The designed inhibitor was also buried in the active site due to bending of the alkyl chain. The R_2 substitution showed interaction with Gly32 at the mouth of the pocket leading to proper orientation thus further adding to the success of the design. The docked designed inhibitors when correlated with the CoMFA, COMSIA maps showed improved correlation.
7. ***Synthetic feasibility:*** The basic scaffold has been adopted from the parent scaffold of dataset for molecules **4**, **21**, **22**. Since the basic template was adopted from the study dataset which was synthesized, the synthetic feasibility of the template is not a problem. The synthetic feasibility of the designed molecules therefore depends on the substitutions. The substitutions are made at eight places (Table 5). On observation of the position of substitution and the relevant molecule, the substitutions were crudely divided into four groups (Gp). With experience it can be easily manifested that Gp 1. substitution can

Table 5 Designed ligands using **4**, **21** and **22** compounds as templates

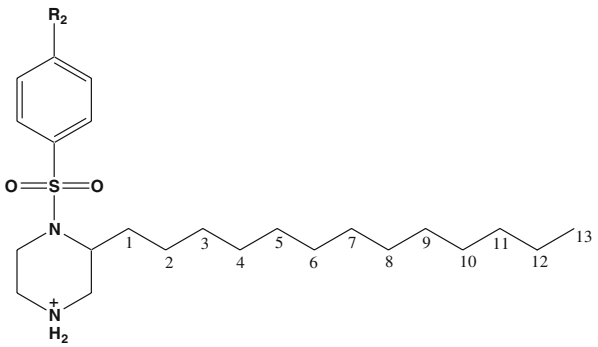

Mol. No.	Name	4	6	8	9	10	11	12	R_2
1.	**4A**	-	-	-	$CH(CH_3)$	-	-	-	-
2.	**4B**	-	-	-	-	$CH(CH_3)$	-	-	-
3.	**4C**	-	-	-	-	-	$CH(CH_3)$	-	-
4.	**4D**	-	-	-	-	-	-	$CH(CH_3)$	-
5.	**4E**	-	-	-	-	-	$CH(C_2H_5)$	-	-
6.	**4F**	-	-	-	-	-	$C(CH_3)_2$	-	-
7.	**4G**	-	-	-	-	-	-	-	$CONH_2$
8.	**4H**	-	-	-	-	-	-	-	$NHCONH_2$
9.	**4I**	-	-	-	-	-	-	-	CH_2CONH_2
10.	**4J**	-	-	-	-	-	-	-	$CH_2NHCOCH_3$
11.	**4AI**	CO	-	-	-	$CH(CH_3)$	-	-	-
12.	**4AIE**	CO	-	-	-	$CH(C_2H_5)$	-	-	-
13.	**4AII**	CO	CO	-	-	$CH(CH_3)$	-	-	-
14.	**4AIIE**	CO	CO	-	-	$CH(C_2H_5)$	-	-	-
15.	**4AIIEE**	CO	CO	$CH(C_2H_5)$	-	$CH(C_2H_5)$	-	-	-
16.	**4AII_nSC**	CO	CO	$CH(CH_3)$	-	$CH(CH_3)$	-	-a-	-
17.	**4AIII**	CO	CO	CO	-	$CH(CH_3)$	-	-	-
18.	**4AIIIE**	CO	CO	CO	-	$CH(C_2H_5)$	-	-	-
19.	**4AIII_n**	CO	CO	$CH(CH_3)$	-	$CH(CH_3)$	-	-	-
20.	**4AIIIE_n**	CO	CO	$CH(CH_3)$	-	$CH(C_2H_5)$	-	-	-
21.	**4AIIIE_nSC**	CO	CO	$CH(CH_3)$	-	$CH(C_2H_5)$	-	-a-	-
22.	**21A**	CO	-	-	-	-	-	-	-
23.	**21B**	CO	CO	CO	-	-	-	-	-
24.	**21C**	CO	CO	CO	NH	-	-	-	-
25.	**21D**	-	-	-	-	-	-	$C(CH_3)_3$	-
26.	**22A**	CO	-	-	-	-	-	-	-
27.	**22B**	CO	CO	CO	-	-	-	-	-
28.	**22C**	CO	CO	CO	NH	-	-	-	-
29.	**22D**	-	-	-	-	-	-	$C(CH_3)_3$	-

- no change; -a- removed from the original template

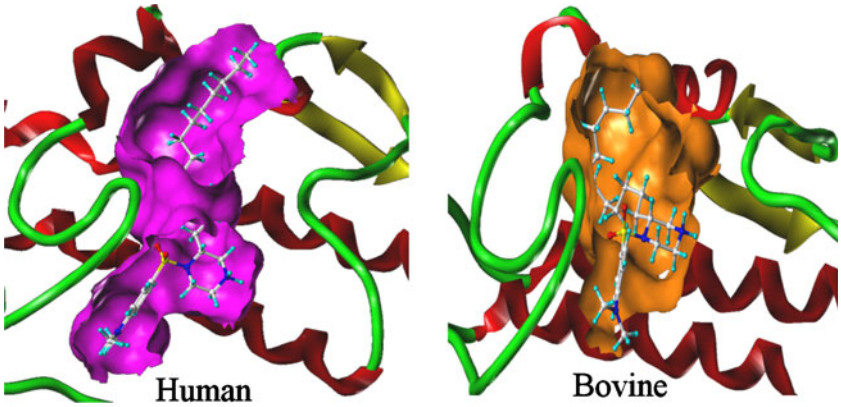

Fig. 9 Docked pose of molecule **21** is displayed in the active sites of human and bovine PLA_2s. The ligand folds to bind deep in the active site pocket of bovine in contrast to human where it does not binds deeply thereby not occupying the hydrophobic pocket of the active site

be brought about by simple oxidation while alkylation is a favorable option for Gp 2. substituted molecules. The Gp 3. substitutions can be synthesized by oxidation followed by condensation whereas Gp 4. substituted molecules need nucleophilic substitution. The substitutions made at the R_1 and R_2 positions are thus synthetically feasible. The details of the same are given in the supporting information.

8. ***Druglike properties:*** As a step further in validating the designed molecules the druglike properties of the molecules have been calculated [36, 37]. The designed molecules successfully satisfy the Lipinski's rule and other necessary parameters to qualify it as a drug (Table 7).

Conclusions

A systematic integration of structure and analog based approaches to model the structural features responsible for PLA_2 inhibitory activities of 1-arylsulfamido-2-alkylpiperazine analogues has been done. The critical analysis reveals that the observed biological activity depends more on the length of the carbon chain. Excellent r^2 and q^2 values were

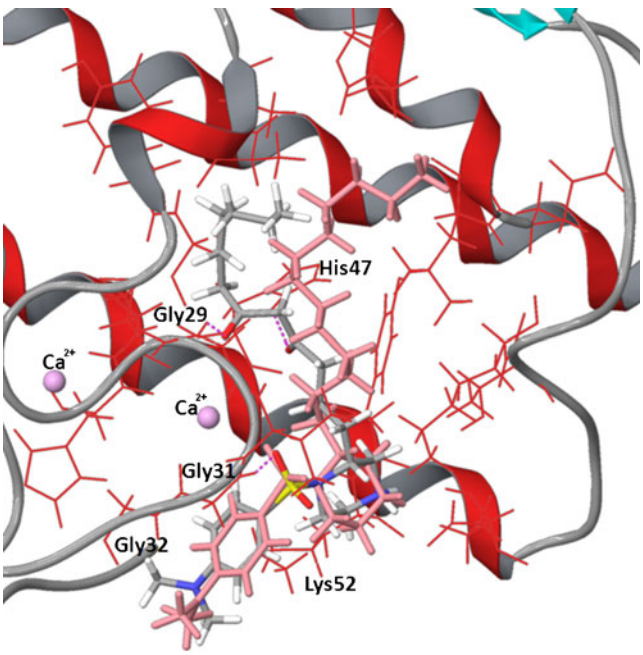

Fig. 10 Docked poses of **21** (pink) and **21B** (atom color) in the active site of human PLA_2. Hydrogen bonds between R_1 substitutions of **21B** with Gly29 and His47 are displayed as red dotted lines which were not observed for **21**. Compared to **21**, **21B** was bound deep inside the pocket. Important active site residues are represented in red lines and calcium as pink color ball

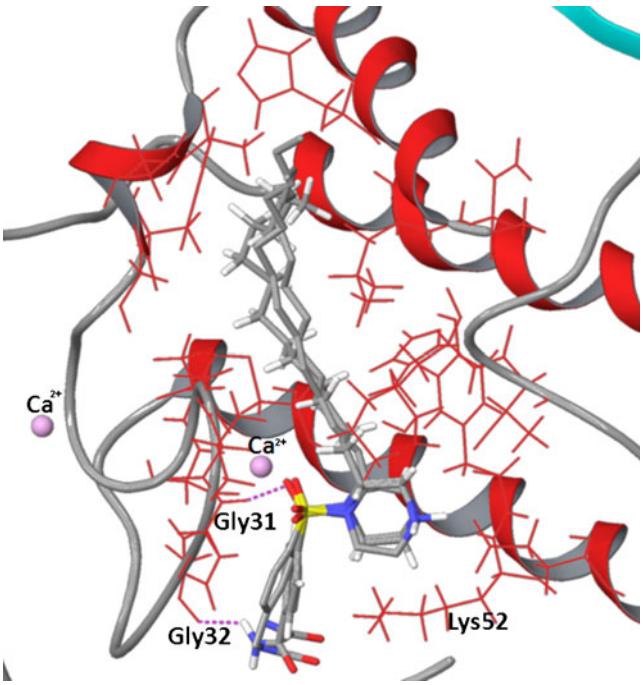

Fig. 11 Docked poses of 4G-J in the active site of human PLA_2. Hydrogen bond between R_2 substitutions with Gly32 is displayed as red dotted lines, which were not observed in the templates. Important active site residues are represented in red lines and calcium as pink color ball

Table 6 GOLD docking scores for designed ligands docked in the active sites of both bovine and human PLA_2s. For comparison the templates were also docked along with designed ligands with the scores given below

Mol. No.	Name	Bovine	Human
1	4	64.55	63.19
2	4A	63.83	58.41
3	4B	57.54	48.17
4	4C	63.24	55.70
5	4D	51.09	53.17
6	4E	54.28	56.06
7	4F	51.36	54.97
8	4G	68.91	57.12
9	4H	65.91	56.59
10	4I	58.22	62.23
11	4J	67.02	58.27
12	4AI	68.35	55.68
13	4AIE	71.15	58.35
14	4AII	76.48	60.20
15	4AIIE	71.52	57.29
16	4AII_n	72.98	58.90
17	4AII_nSC	70.07	55.67
18	4AIII	83.67	70.78
19	4AIIIE	76.20	63.36
20	4AIIIEE	52.83	58.62
21	4AIIIE _n	68.9	54.80
22	4AIIIE_nSC	76.83	63.99
23	21	62.42	48.90
24	21A	55.74	52.03
25	21B	55.10	64.07
26	21C	54.30	56.74
27	21D	47.29	47.50
28	22	52.87	54.62
29	22A	71.88	57.96
30	22B	73.57	65.27
31	22C	69.44	66.02
32	22D	46.04	50.03

Table 7 Listing of druglike properties of the designed molecules for human secreted PLA_2

Mol. No.	Name	Lipinski's druglike properties			
		H-bond donors	H-bond acceptors	Mol. Wt.	LogP
1	4A	2	1	451.72	2.677
2	4B	2	1	451.72	2.537
3	4C	2	1	437.70	2.711
4	4D	2	1	437.70	2.855
5	4E	2	1	437.70	2.834
6	4F	2	1	437.70	3.016
7	4G	3	2	452.67	0.999
8	4H	3	3	467.68	1.264
9	4I	3	2	466.70	1.413
10	4J	3	2	480.72	1.851
11	4AI	3	1	451.68	1.746
12	4AIE	3	1	465.71	1.881
13	4AII	4	1	465.66	0.658
14	4AIIE	4	1	479.69	0.971
15	4AIIEE	4	1	507.74	1.280
16	4AII_nSC	4	1	451.64	0.254
17	4AIII	5	1	493.67	0.147
18	4AIIIE	4	1	491.70	0.456
19	4AIII_n	4	1	463.65	0.413
20	4AIIIE_n	5	1	479.65	1.030
21	4AIIIE_nSC	2	1	423.67	0.364
22	21A	4	1	466.70	1.869
23	21B	6	1	494.66	−0.109
24	21C	6	2	495.65	−0.720
25	21D	3	1	480.70	3.257
26	22A	3	2	494.75	0.839
27	22B	4	2	480.68	−1.028
28	22C	6	2	508.65	−1.528
29	22D	6	3	509.63	2.188

obtained for the 3D-QSAR employed, indicating that the models constructed have good correlations and predictive properties. Predictive power of CoMFA and CoMSIA models was evaluated by the test set and good predictive r^2 values were obtained. The docking analysis has provided a qualitative representation of ligand-protein interactions, which were not only correlating with the reported experimental results but were also complementary with the CoMFA and CoMSIA maps. The 3D-QSAR and docking studies indicate that the optimum chain length could be in between C_9 to C_{12} to facilitate SO_2 group interactions with the metal and phenyl ring with the solvent. The 29 new inhibitors were designed based on the clues and understanding from the various molecular modeling studies performed. The molecules with C_{12} chain as templates on basis of docking results. The combined analysis of the QSAR and docking results put together warranted the addition of long chain alkyl groups with small alkyl and carboxyl groups substituted on different carbons of alkyl chain so as to facilitate bending of chain on the formation of bonds with the surrounding Gly 29, Gly31, Gly32, Glu55 and Lys 62 leading to the proper occupancy of active site. With the success rendered by the *in silico* validation the possibility on the synthesis of these designed inhibitors was pondered upon. Although the designed inhibitors were not synthesized, the synthetic feasibility of the various groups substituted has been

considered. The study enunciates the use of QSAR and docking protocols for the *in silico* design of new leads with better affinity and experimental validation of these predictions are very desirable. The main idea is to decipher different ways for *in silico* design of inhibitor for a chosen therapeutic target by rational application of molecular modeling protocols. The elegant complementary of the analog and structure based approaches found to provide valuable insights into the ligand interactions at the receptor, which eventually enhances understanding of the structural requirements for the design of novel and potential PLA_2 inhibitors. This approach, a prelude to synthesis and biological testing is expected to cut down on time and increase success rate. We hope that honing the development of such strategies will cause a paradigm shift in drug discovery.

Acknowledgments Department of Biotechnology (DBT), New Delhi is thanked for the financial support. DST is thanked for the women scientist award to PB and Swarnajayanthi Fellowship to GNS.

References

1. Heinrikson RL, Krueger ET, Keim PS (1977) Amino acid sequence of phospholipase A_2-alpha from the venom of Crotalus adamanteus. A new classification of phospholipases A_2 based upon structural determinants. J Biol Chem 252:4913–4921
2. Waite M (ed) (1987) The phospholipases in handbook of lipid research. Plenum, New York, pp 1–332
3. Valentin E, Lambeau G (2000) Increasing molecular diversity of secreted phospholipase A_2 and their receptor and protein binding proteins. Biochim Biophys Acta — Mol Cell Bio Lip 1488:59–70
4. Dennis EA (1994) Diversity of group types, regulation, and function of phospholipase A_2. J Biol Chem 269:13057–13060
5. Uhl W, Nevalainen TJ, Buchler MW (eds) (1997) Phospholipase A_2: basic and clinical aspects in inflammatory diseases. Karger, Basel
6. Kovanen PT, Pentikainen MO (2000) Secretory group II phospholipase A_2: a newly recognized acute-phase reactant with a role in atherogenesis. Circ Res 86:610–612
7. Forster S, Ilderton E, Norris JFB, Summerly R, Yardley HJ (1985) Characterization and activity of phospholipase A_2 in normal human epidermis and in lesion-free epidermis of patients with psoriasis or eczema. Br J Dermatol 112:135–147
8. Minami T, Tojo H, Shinomura Y, Matsuzawa Y, Okamoto M (1994) Increased group II phospholipase A_2 in colonic mucosa of patients with Crohn's disease and ulcerative colitis. Gut 35:1593–1598
9. Meyer MC, Rastogi P, Beckett CS, McHowat J (2005) Phospholipase A_2 inhibitors as potential anti-inflammatory agents. Curr Pharm Des 11:1301–1312
10. Dong CZ, Himidi AA, Plocki S, Aoun D, Touaibia M, Habich NM, Huet J, Redeuilh C, Ombetta JE, Godfroid JJ, Massicota F, Heymans F (2005) Bioorg Med Chem 13:1989–2007
11. Jabeen T, Singh N, Singh RK, Sharma S, Somvanshi RK, Dey S, Singh TP (2005) Non-steroidal anti-inflammatory drugs as potent inhibitors of phospholipase A_2: structure of the complex of phospholipase A_2 with niflumic acid at 2.5 angstroms resolution. Acta Crystallogr D Biol Crystallogr 61:1579–1586
12. Muller P, Lena G, Boilard E, Bezzine S, Lambeau G, Guichard G, Rognan D (2006) In silico-guided target identification of a scaffold-focused library: 1, 3, 5-triazepan-2, 6-diones as novel phospholipase A2 inhibitors. J Med Chem 49:6768–6778
13. Dillard RD, Bach NJ, Draheim SE, Berry DR, Carlson DG, Chirgadze NY, Clawson DK, Hartley LW, Johnson LM, Jones ND, McKinney ER, Mihelich ED, Olkowski JL, Schevitz RW, Smith AC, Snyder DW, Sommers CD, Wery J-P (1996) Indole inhibitors of human nonpancreatic secretory phospholipase A_2. 1. Indole-3-acetamides. J Med Chem 39:5119–5136
14. Dillard RD, Bach NJ, Draheim SE, Berry DR, Carlson DG, Chirgadze NY, Clawson DK, Hartley LW, Johnson LM, Jones ND, McKinney ER, Mihelich ED, Olkowski JL, Schevitz RW, Smith AC, Snyder DW, Sommers CD, Wery J-P (1996) Indole inhibitors of human nonpancreatic secretory phospholipase A_2. 2. Indole-3-acetamides with additional functionality. J Med Chem 39:5137–5158
15. Draheim SE, Bach NJ, Dillard RD, Berry DR, Carlson DG, Chirgadze NY, Clawson DK, Hartley LW, Johnson LM, Jones ND, McKinney ER, Mihelich ED, Olkowski JL, Schevitz RW, Smith AC, Snyder DW, Sommers CD, Wery J-P (1996) Indole inhibitors of human nonpancreatic secretory phospholipase A_2. 3. Indole-3-glyoxamides. J Med Chem 39:5159–5175
16. Bernard P, Pintore M, Berthon JY, Chretien JR (2001) A molecular modeling and 3D QSAR study of a large series of indole inhibitors of human non-pancreatic secretory phospholipase A_2. Eur J Med Chem 36:1–19
17. Binisti C, Assogba L, Touboul E, Mounier C, Huet J, Ombetta JE, Dong CZ, Redeuilh C, Heymans F, Goldfroid JJ (2001) Structure—activity relationships in platelet-activating factor (PAF). 11-From PAF-antagonism to phospholipase A_2 inhibition: syntheses and structure—activity relationships in 1-arylsulfamido-2-alkylpiperazines. Eur J Med Chem 36:809–828
18. Cramer RD, Patterson DE, Bunce JD (1988) Comparative molecular field analysis (CoMFA). 1. Effect of shape on binding of steroids to carrier proteins. J Am Chem Soc 110: 5959–5967
19. Klebe G, Abraham U, Mietzner T (1994) Molecular similarity indices in a comparative analysis (CoMSIA) of drug molecules to correlate and predict their biological activity. J Med Chem 37:4130–4146
20. Vellarkad N, Viswanadhan VN, Ghose AK, Revenkar R, Robins RN (1989) Atomic physicochemical parameters for three dimensional structure directed quantitative structure-activity relationships. 4. Additional parameters for hydrophobic and dispersive interactions and their application for an automated superposition of certain naturally occurring nucleoside antibiotics. J Chem Inf Comput Sci 29:163–172
21. Srivani P, Kiran K, Sastry GN (2006) Understanding the structural requirements of triarylethane analogues towards PDE IV inhibitors: a molecular modeling study. Ind J Chem A 45A:68–76
22. Janardhan S, Srivani P, Sastry GN (2006) 2D and 3D quantitative structure-activity relationship studies on a series of *bis*-pyridinium compounds as choline kinase inhibitors. QSAR Comb Sci 25:860–872
23. Srivani P, Srinivas E, Raghu R, Sastry GN (2007) Molecular modeling studies of pyridopurinone derivatives — Potential phosphodiesterase 5 Inhibitors. J Mol Graph Model 26:378–390
24. Kulkarni RG, Srivani P, Achaiah G, Sastry GN (2007) Strategies to design of pyrazolyl urea derivatives for p38 kinase inhibition: a molecular modeling study. J Comput Aided Mol Design 25:155–166
25. Kulkarni RG, Achaiah G, Sastry GN (2008) Molecular modeling studies of phenoxypyrimidinyl imidazoles as p38

kinase inhibitors using QSAR and docking. Eur J Med Chem 43:830–838
26. Srivani P, Sastry GN (2009) Potential choline kinase inhibitors: a molecular modeling study of bis-quinolinium compounds. J Mol Graph Model 27:676–688
27. SYBYL 6.9. Molecular Modeling Software, Tripos Inc, 1699 Hanley Road, St Louis, MO 63144
28. Rarey M, Kramer B, Lengauer T, Klebe G (1996) A fast flexible docking method using an incremental construction algorithm. J Mol Biol 261:470–489
29. GOLD, version 2.1; Cambridge Crystallographic Data Centre: Cambridge, UK
30. Jones G, Willet P, Glen RC, Leach AR, Taylor R (1997) Development and validation of a genetic algorithm for flexible docking. J Mol Biol 267:727–748
31. Reddy AS, Priyadarshini PS, Kumar PP, Pradeep HN, Sastry GN (2007) Virtual screening in drug discovery — A computational perspective. Curr Prot Pept Sci 8:329–351
32. Jin ZM, Pan YJ, He L, Li ZG, Yu KB (2003) Crystal structure of the 1:2:2 adduct of piperazine, o-phthalic acid and water. Anal Sci 19:333–334
33. Coupar PI, Ferguson G, Glidewell C (1996) Piperazine-4, 4′-sulfonyldiphenol (1/2): a self-assembled channel structure. Acta Crystallogr 52:3052–3055
34. Wouters J, Haming L, Sheldrick G (1996) HEPES. Acta Crystallogr 52:1687–1688
35. Thompson JD, Higgins DG, Gibson TJ (1994) CLUSTAL W: improving the sensitivity of progressive multiple sequence alignment through sequence weighting, position-specific gap penalties and weight matrix choice. Nucleic Acids Res 22:4673–4680
36. Alessandro P, Vistoli G, Gaillard P, Carrupt PA, Testa B, Boudon A (1994) Molecular lipophilicity potential, a tool in 3D QSAR: method and applications. J Comput Aided Mol Des 8:83–96
37. Accelrys Discovery Studio v2.1.0.8130